THE JOURNAL OF PHYSICAL CHEMISTRY C

Article

pubs.acs.org/JPCC

High Stability and Ultralow Threshold Amplified Spontaneous Emission from Formamidinium Lead Halide Perovskite Films

Fang Yuan,[†] Zhaoxin Wu,*[,†] Hua Dong,[†] Jun Xi,[†] Kai Xi,[§] Giorgio Divitini,[§] Bo Jiao,[†] Xun Hou,[†] Shufeng Wang,[‡] and Qihuang Gong[‡]

[†]Key Laboratory of Photonics Technology for Information, Key Laboratory for Physical Electronics and Devices of the Ministry of Education, School of Electronic and Information Engineering, Xi'an Jiaotong University, Xi'an 710049, P. R. China

[‡]State Key Laboratory for Mesoscopic Physics and Department of Physics, Peking University, Beijing 100871, P. R. China

[§]Department of Materials Science and Metallurgy, University of Cambridge, Cambridge CB3 0FS, U.K.

Supporting Information

ABSTRACT: The opportunity of lasing from organolead halide perovskite materials has recently attracted extensive attention in order to realize electrically driven lasers. So far, for devices with planar structure, most reports focus on $CH_3NH_3PbI_3$ ($MAPbI_3$) films, which are unstable when in operation due to phase transitions and elemental redistribution. Herein, we demonstrate highly stable amplified spontaneous emission (ASE) with ultralow threshold from formamidinium-based perovskite $CH(NH_2)_2PbI_3$ ($FAPbI_3$) films. ASE from MABr-stabilized $FAPbI_3$ films was also achieved, with an ultralow threshold of about 1.6 $\mu J/cm^2$. More importantly, upon continuous operation under pulsed laser for several hours, the ASE intensity in the $MAPbI_3$ film decreased to 9% of the initial value, while it was maintained above 90% in the $FAPbI_3$ film. The low trap density, smooth film morphology, high thermal stability, and the excitonic emission in nature of the $FAPbI_3$ film are expected to contribute to its low lasing threshold and high stability, demonstrating a strong potential for applications in continuous-wave pumped lasers and electrically driven lasers.

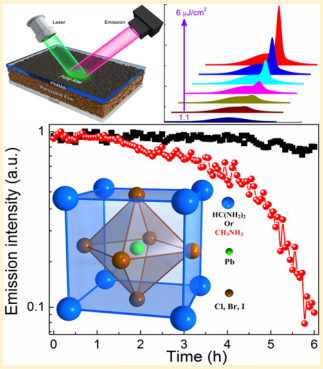

1. INTRODUCTION

In the past few years, hybrid halide perovskites, with the general formula ABX_3 (where A for $CH_3NH_3^+$ or $HC(NH_2)_2^+$ cation; B for Sn^{2+} or Pb^{2+} metal ion; and X for I, Br, Cl), have been at the basis of several breakthroughs in photovoltaic and optoelectronic applications.[1−6] Employed as light absorbers in solar cells, rapid improvements in the power conversion efficiency (PCE) have been achieved,[7−9] thanks to a combination of broadband absorption, balanced charge transport properties with long diffusion lengths, and low nonradiative recombination ascribed to their unique defect chemistry.[1,2,10−12] Current state-of-the-art solar cells based on perovskite materials achieved a certified PCE of 22.1%.[13] Meanwhile, the demonstration of high photoluminescence (PL) quantum efficiency and optical gain in these hybrid perovskites suggests that these materials should also be effective light emitters for light-emitting diodes and lasers which can be easily tuned across the entire visible spectrum via halogen substitutions.[3−5,14,15]

Considering the balanced ambipolar charge transport and high gain characteristics of $CH_3NH_3PbX_3$ ($MAPbX_3$ in the following text), these hybrid perovskite materials show promising prospect for electrically pumped lasers. So far, optically pumped amplified spontaneous emission (ASE) as well as lasing have been demonstrated in a variety of sample morphologies such as polycrystalline thin films,[15−17] microcavity,[18,19] nanocrystals,[20] nanowires,[21−23] and distributed feedback cavity.[24] Although the reported thresholds are very promising, major challenges still prevent the use of perovskite-based electrically pumped lasers. One major obstacle for practical applications is the instability that stems from poor thermal stability and high moisture sensitivity of the perovskite film.[25] In particular, the thermal stability may impose technical limits for the realization of electrically driven lasers, since the heating caused by the large current injection could potentially cause the degradation of perovskite materials.[15,26] Moreover, $MAPbI_3$ undergoes a reversible phase transition between tetragonal and cubic phase at ∼330 K,[27,28] a temperature that might be achieved in an operating optoelectronic device, and the phase transition can modify the emission properties of $MAPbI_3$. In addition, a lower current density threshold estimated from the optically pumped threshold is desirable, which means that achieving a low-threshold optically pumped laser system is a motivating goal, as it lowers the amount of pump energy necessary to drive the laser. With a long-term view, an electrically pumped laser would be also obviously demonstrated more easily in a low threshold structure. Therefore, materials with high stability and low gain threshold are desirable for the realization of electrically driven lasers.

Received: March 5, 2017
Revised: May 28, 2017
Published: July 3, 2017

DOI: 10.1021/acs.jpcc.7b02101
J. Phys. Chem. C 2017, 121, 15318−15325

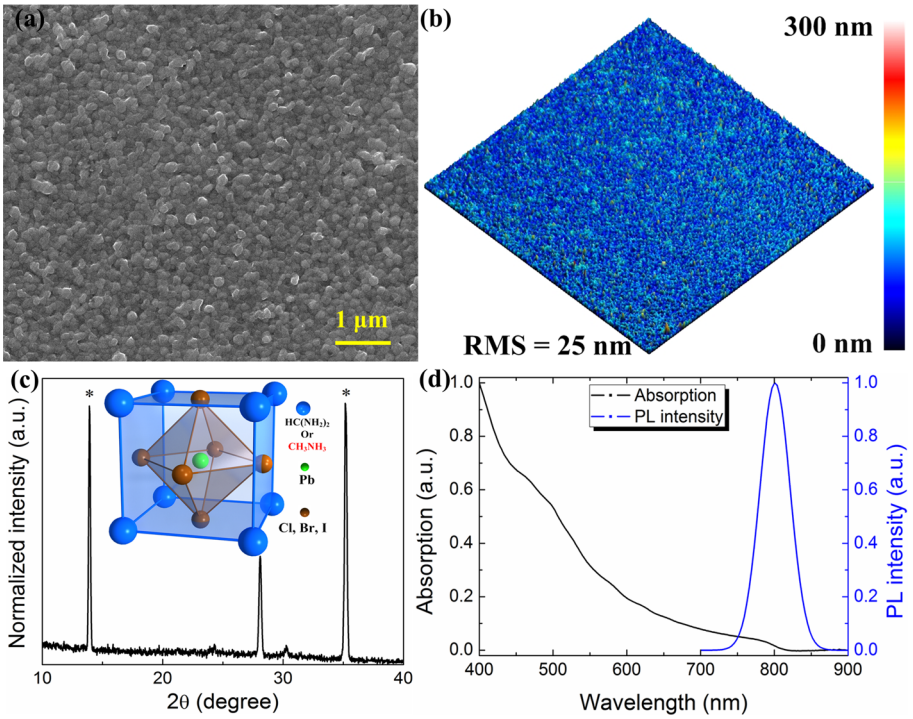

Figure 1. $FAPbI_3$ film characterization. (a) Top view SEM image of the $FAPbI_3$ film. (b) 3D AFM image of the $FAPbI_3$ film. (c) Bragg−Brentano X-ray diffraction pattern for a typical $FAPbI_3$ film. The main diffraction peaks are labeled with black stars. The inset shows the atomic crystal structure of $FAPbI_3$ and $MAPbI_3$. (d) Normalized absorption spectrum and PL spectrum of the $FAPbI_3$ film.

In this work, we report the ASE in the optically pumped $HC(NH_2)_2PbI_3$ (shortened as $FAPbI_3$) and MABr-stabilized $FAPbI_3$ films, possessing an ultralow threshold of about 1.6 $\mu J/cm^2$. We further demonstrate tunable perovskite ASE in wider wavelength region from FA-based lead halide perovskite alloys through halogen substitutions. Remarkably, upon pumping with pulsed laser for hours, the $FAPbI_3$ film displays more durable lasing emission than $MAPbI_3$. In addition, temperature-dependent PL experiments reveal an exciton binding energy of 29 meV and optical phonon energy of 19 meV, indicating an excitonic emission in nature at room temperature. The improvements in low lasing threshold and high stability in the $FAPbI_3$ film were expected to stem from its low trap density, smooth film morphology, high thermal stability, and the excitonic emission in nature.

2. EXPERIMENTAL METHODS

Sample Preparation. To prepare the samples, the precleaved glass substrates were cleaned with deionized water and organic solvents and then exposed to a UV−ozone ambient for 5 min. Then, the $FAPbI_3$ layer was fabricated in N_2 ambient glovebox as follows: Lead iodide (PbI_2, Sigma-Aldrich, 99.999%) and formamidinium iodide ($CH(NH_2)_2I$, or FAI) were dissolved in anhydrous dimethylformamide (DMF) and 2-propanol, respectively. The PbI_2/DMF precursor solution (369.6 mg/mL) was deposited onto a hot plate at 60 °C with stirring and was maintained at 60 °C before spin coating on substrates to keep its viscosity at an optimized range. Then the PbI_2/DMF solution was spin-coated at 6000 rpm for 60 s onto the substrate and then annealed at 100 °C for 10 min to thoroughly remove the DMF residue. Then 0.4 mL of FAI precursor solution (10.84 mg/mL) was spin-coated at 2000 rpm for 30 s onto the mentioned substrate with PbI_2 (90 nm) all at 60 °C and then annealed at 120 °C for 20 min to form the perovskite layer. For comparison, the $MAPbI_3$ film was prepared via the same method by spin-coating the MAI isopropyl alcohol solution (10 mg/mL) onto the mentioned PbI_2 substrate and then annealed at 100 °C for 20 min to form the perovskite layer. Finally, poly(methyl methacrylate) (PMMA) dissolved in the chlorobenzene solution (20 mg/mL) was spin-coated at 1000 rpm for 30 s onto the substrate and then annealed at 100 °C for 10 min to complete device preparation. The PMMA films were spin-coated as encapsulated layer to protect the $FAPbI_3$ layer from degradation by moisture and oxygen in atmospheric environment. The perovskite film double alloys of $(MA,FA)Pb(Br,I)_3$ were prepared by reacting PbI_2 film with different ratio FAI and MABr in isopropanol ranging from 1:0 to 0:1.

Sample Characterization. Film thickness of the samples was measured by ellipsometry (SE MF-1000, Korea). The surface of $MAPbI_3$ layer was investigated by scanning electron microscopy (SEM, Quanta 250, FEI). Surface topography of the $MAPbI_3$ layer was measured by an atomic force microscope (AFM, NT-MDT, Russia). The crystalline structure of the $MAPbI_3$ layer on ITO substrate was determined by X-ray diffraction (XRD, D/MAX-2400, Rigaku, Japan). The absorption and PL spectra were obtained by a UV−vis spectrophotometer (HITACHI U-3010, Japan) and a fluorescence spectrometer (Fluoromax-4 spectrofluometer), respectively. The femtosecond pulses were delivered from the frequency-doubled output of a Ti:sapphire femtosecond laser oscillator. The nanosecond pulses were delivered by a frequency-doubled Nd:YAG laser (Surelite I, Continuum Corp., USA). Face emission spectra were collected by a fiber-optic spectrometer (Ocean Optics SpectraSuite, USB2000).

DOI: 10.1021/acs.jpcc.7b02101
J. Phys. Chem. C 2017, 121, 15318−15325

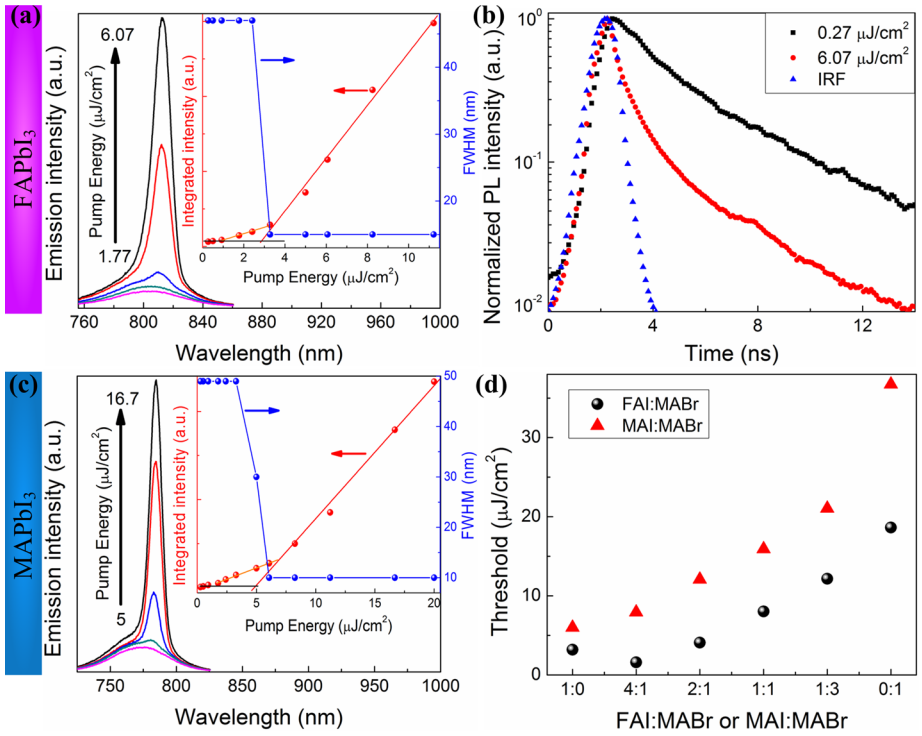

Figure 2. (a) Face emission spectra of $FAPbI_3$ film pumped by pulsed laser with duration of 150 fs. The insets show the integrated emission intensity and the fwhm of the face emission spectra as a function of pump energy. (b) Time-resolved PL decay kinetics of $FAPbI_3$ film below (black squares) and above (red circles) ASE threshold. Also shown in blue triangle is the instrument response function. (c) Face emission spectra of $MAPbI_3$ film pumped by a femtosecond pulsed laser. The insets show the integrated emission intensity and the fwhm of the face emission spectra as a function of pump energy. (d) Wavelength-tunable lasing thresholds achieved by both cation and anion substitutions.

3. RESULTS AND DISCUSSION

To prepare the samples, the hot PbI_2/DMF precursor solution (369.6 mg/mL, 60 °C) was spin-coated onto the preclean glass substrate and then annealed. Then 0.4 mL of FAI isopropyl alcohol solution (10.84 mg/mL) was spin-coated onto the mentioned substrate with PbI_2 (90 nm), all at 60 °C, and then annealed at 120 °C for 20 min in N_2 ambient inside a glovebox. The two stacked precursor layers start forming after deposition and their structure is fully crystallized via thermal annealing to form the perovskite layer through the interdiffusion process.[29] For comparison, the $MAPbI_3$ film was prepared via the same method, by spin-coating the MAI isopropyl alcohol solution (10 mg/mL) onto the mentioned PbI_2 substrate. PMMA films were spin-coated as encapsulating layer to protect the perovskite films from degradation by moisture and oxygen in atmospheric environment (see Experimental Methods). All measurements were carried out under ambient conditions at room temperature.

A scanning electron micrograph (SEM) of the top surface of the $FAPbI_3$ film is presented in Figure 1a. The as-formed $FAPbI_3$ film has full surface coverage on the substrates, with a grain size of about 110−150 nm, which is slightly smaller than the grain size of $MAPbI_3$ grown in the same conditions (Figure S1, Supporting Information). The 3D surface topography of the $FAPbI_3$ film is further evaluated by atomic force microscope (AFM) as shown in Figure 1b. The $FAPbI_3$ film is relatively smooth compared to other solution-processed films, with the root-mean-square (RMS) of surface roughness about 25 nm over the measured area of 50 μm × 50 μm. Figure 1c shows the corresponding X-ray diffraction (XRD) of the as-prepared $FAPbI_3$ film on glass substrate. A set of strong peaks at 13.94°, 28.12°, and 35.21°, assigned to (110), (220), and (312) of the $FAPbI_3$ crystal, indicates a trigonal crystal structure of halide perovskite with high crystallinity. The normalized optical absorption and PL spectra from the $FAPbI_3$ film are shown in Figure 1d. The energy gap extracted from the absorption spectra is about 1.55 eV, which is in good agreement with PL spectra exhibiting a SE peak at 801 nm, with the full width at half-maximum (fwhm) about 51 nm. By contrast, the energy gap of $MAPbI_3$ film is larger, with a PL peak at 765 nm (Figure S2).

The samples were excited at 400 nm by a frequency-doubled Ti:sapphire femtosecond laser oscillator delivering 150 fs pulses at a 1 kHz repetition rate. Through a pinhole filter and a positive lens, the laser beam formed a 3 mm diameter spot and was irradiated obliquely onto the surface of the samples (Figure S3). Face emission spectra were collected directly into a fiber optic spectrometer. The measured output emission spectra, input−output intensity, and fwhm of the sample as a function of increasing pump energy are shown in Figure 2. The evolution of light emission spectra from the $FAPbI_3$ film is illustrated in Figure 2a, showing the transition from the SE to ASE with increasing pump energy. Clearly, as shown in the inset of Figure 2a, there is a visible threshold at about 3 ± 0.5 μJ/cm^2 in the input−output curve. At low pump energy, only a SE peak is observed. When the pump intensity exceeds the threshold, the spectral narrowing, i.e., ASE, emerges at 812 nm while the fwhm dramatically decreased from ∼47 to ∼15 nm. The fwhm remains constant upon further increase in the pump energy. ASE can be achieved in the $FAPbI_3$ film because the spontaneously emitted photons transmitted along the gain media are amplified by stimulated emission. Owing to the stronger self-absorption, ASE does not occur at the SE peak

DOI: 10.1021/acs.jpcc.7b02101
J. Phys. Chem. C 2017, 121, 15318−15325

wavelength 801 nm but 812 nm, where the optical gain and absorption are balanced. Another characteristic and expected feature of ASE, seen in time-resolved experiments (Figure 2b), is the acceleration of radiative recombination due to switching from individual to collective emission. For $FAPbI_3$ films in this work, at excitation intensities lower than the ASE threshold, typical PL lifetimes of several nanoseconds are observed with nearly single-exponential behavior (Figure 2b, black squares). Well above the ASE threshold, an ASE lifetime of few hundred picoseconds, limited by instrument resolution, can be roughly estimated from a biexponential fit, assuming competing ASE and PL processes (Figure 2b, red circles). In addition, the first intersection shown in the inset of Figure 2a represents the pump energy needed to fill all the traps (i.e., the threshold trap pump energy P_{th}^{Trap}). $P_{th}^{Trap} \sim 1\ \mu J/cm^2$ is shown in the input−output curve, corresponding to a trap state density of about $10^{17}\ cm^{-3}$. By contrast, the $MAPbI_3$ film possesses a higher threshold—about 6 $\mu J/cm^2$—than the $FAPbI_3$ film, which indicates a higher trap state density, about $2.5 \times 10^{17}\ cm^{-3}$, as clearly shown in Figure 2c. In addition, we grow perovskite film double alloys of $(MA,FA)Pb(Br,I)_3$ by reacting PbI_2 film with a mixed solution of FAI and MABr in isopropanol (Figure S4) to achieve wavelength-tunable lasing from 820 to 615 nm (Figure S5). The thresholds increase with the increasing proportion of MABr, ranging from about 1.6 to 37 $\mu J/cm^2$, as shown in Figure 2d. It is worth to mention that a threshold as low as 1.6 $\mu J/cm^2$ is achived in the perovskite film for FAI:MABr = 4:1, which probably is enabled by the smooth film morphology and the low trap state density (Figure S6). Furthermore, appropriate proportion of MABr and FAI in the PbI_2 skeleton could improve the phase stability of $FAPbI_3$,[9,30] which is also beneficial to the improved luminescence properties of the MABr-stabilized $FAPbI_3$ films.

A quasi-continuous wave regime of excitation can be observed with pumping pulses of longer duration than the ASE lifetime, though at the expense of higher overall pumping energy to maintain the same instant excitation intensity over the whole pulse duration. In order to further investigate the potential for "quasi-continuous wave" regime of excitation, face emission spectra from $FAPbI_3$ film pumped by a nanosecond pulsed laser (532 nm, 5.5 ns, 10 Hz) were obtained with pumping pulses much larger than the ASE lifetime of $FAPbI_3$ (about a few hundred picoseconds). The evolution of light emission spectra is illustrated in Figure 3a, showing a threshold at about 19.5 $\mu J/cm^2$, which validates the potential for employing this material for the realization of continuous-wave (CW) pumped lasers.

For implementing perovskite lasing into optoelectronic devices, the photostability of the emission needs to be assessed. We tested the lasing stability of $FAPbI_3$ and $MAPbI_3$ by pumping them with a 532 nm pulsed laser (5 ns, 10 Hz) at power density above the threshold for several hours. In addition, the photostability of the $FAPbI_3$ and $MAPbI_3$ film was assessed by monitoring the ASE intensity as a function of time under continuous laser pulse 128 $\mu J/cm^2$ for 6 h at room temperature, as shown in Figure 3b. Upon continuously pumping, the ASE intensity in the $MAPbI_3$ film decreased to 9% of the initial value, while it was only mostly retained (90% of the starting value) in the $FAPbI_3$ film. The lack of decay in the emission intensity confirmed the excellent optical stability of the $FAPbI_3$ gain media, which excluded the influence of material degradation or pump energy attenuation on the above-mentioned emission intensity decrease with the continuous

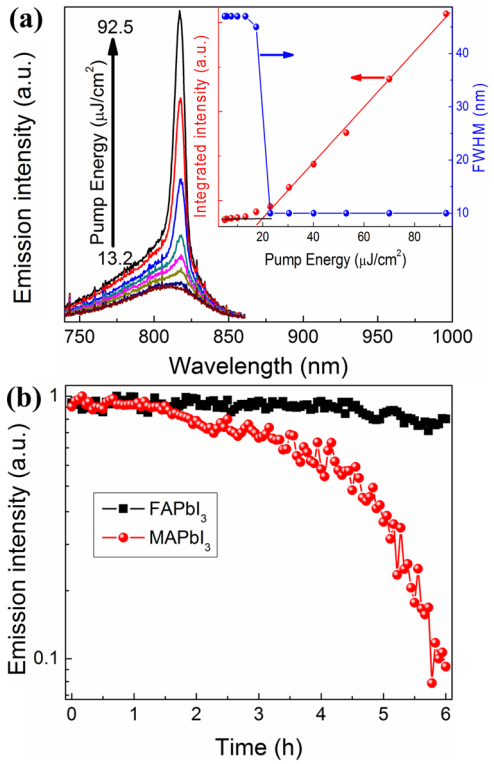

Figure 3. (a) Face emission spectra of $FAPbI_3$ layer pumped by ns pulsed laser. The insets show the integrated emission intensity and the fwhm of the face emission spectra as a function of pump energy. (b) ASE intensity as a function of time under continuous laser pulse at power density above the threshold at room temperature.

laser pulse. We deduced that the improved photostability of $FAPbI_3$ film over $MAPbI_3$ film may derive from two important factors. First, $FAPbI_3$ film is relatively less susceptible to the generated heat induced by sustained laser illumination due to better thermal stability than $MAPbI_3$.[27] Second, the larger FA cation size and the enhanced interaction between FA cations and iodine ions may abate the light-induced ion migration in $FAPbI_3$ film.[31] We should emphasize that the deeper insight into the excellent optical stability of the $FAPbI_3$ film demands further structural and optical investigations, which is beyond the scope of this paper.

To investigate the intrinsic optical properties of different crystalline phase structures of the perovskites films, temperature-dependent PL measurements from 80 to 340 K were carried out, and the data are summarized in Figure 4. The optical excitation is set at low pump energy (0.5 $\mu J/cm^2$) in order to thoroughly comprehend the phase transition in the perovskites in a broad temperature range. As shown in Figure 4a, the temperature-dependent PL emission intensity of the fabricated $FAPbI_3$ film gradually decreases with increase of temperature, indicating thermal quenching of photoinduced charge generation. In a sequence of cooling process from 340 to 80 K, a sharp peak occurs at 140 K, and the corresponding PL emission spectrum is centered at 838 nm. All the PL emission spectra show a blue-shift tendency on their central wavelengths except an obvious variation of the spectral characteristics in a range of temperatures from 120 to 160 K. Such a temperature range of the PL spectral behavior change of $FAPbI_3$ during the temperature-increasing process may refer to a structural phase transition which occurs from hexagonal to trigonal crystalline structure, as described by Kanatzidis et al.,[27] while a recent

DOI: 10.1021/acs.jpcc.7b02101
J. Phys. Chem. C 2017, 121, 15318−15325

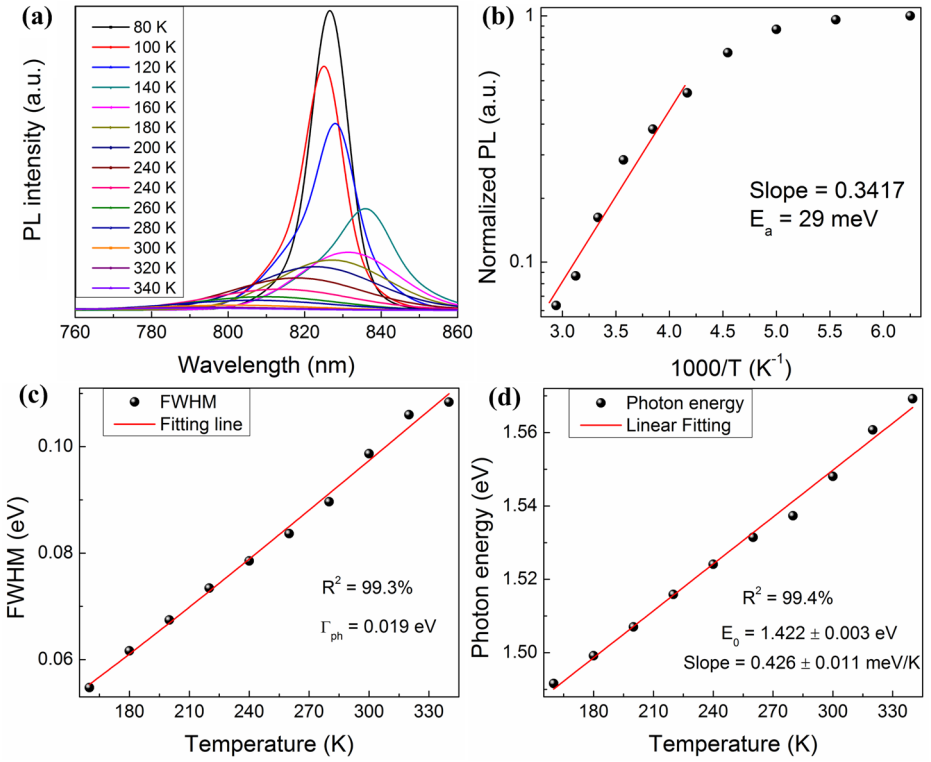

Figure 4. Temperature-dependent PL analysis results for the $FAPbI_3$ film. (a) Temperature-dependent PL spectra taken from 80 to 340 K. (b) Arrhenius plots of the temperature dependence of the integrated PL intensity. The data have been normalized to the intensity at 160 K. The solid lines are linear regressions at high temperatures to extract the values of the activation energies E_a. (c) The spectra fwhm vs temperature for $FAPbI_3$ film. Only the region from 160 to 340 K can be fitted with eq 1 since the material undergoes a phase transition at 160 K. The analysis yields values of 0.019 eV for Γ_{ph}. (d) Temperature-dependent data of the emission peak energy above 160 K. The solid lines are the linear fitting line.

report also revealed a first-order phase transition from tetragonal β-phase to tetragonal γ-phase at around 140 K.[32] Similar evolution of the PL emission spectra in $MAPbI_3$ film with the cooling process from 340 to 80 K is observed, which also show a structural phase transition in a range of temperatures from 120 to 160 K (Figure S7). The structural phase transition from orthorhombic to tetragonal crystalline structures at about 160 K in $MAPbI_3$ film has been observed in some other studies.[33−35]This phase transition in temperature-dependent experiments derives from a tilting of the PbI_6-octahedra out of the *ab*-plane.[35] Similar structural phase transition was also observed in other organic−inorganic lead bromide perovskite microstructures.[36]

As mentioned above, the temperature-dependent PL experiments were performed at very low excitation density under femtosecond laser pulse, which corresponds to the onset of the appearance of the first excited state. The temperature quenching of the PL intensity is due to the thermally activated depopulation of the excitonic level and/or to the activation of nonradiative recombination centers. Since PL intensities are inversely proportional to nonradiative lifetimes $\tau \propto \exp(E_a/kT)$, the activation energies E_a of the processes involved can therefore be determined from the slope of an Arrhenius plot of the integrated PL intensity for the $FAPbI_3$ film as shown in Figure 4b. The shape of these curves is typical of the temperature dependence for semiconductors.[37,38] The regime of strong thermal quenching at high temperatures tends toward a straight line, characteristic of an exponential quenching $\propto \exp(E_a/kT)$. We can deduce the activation energy E_a for the $FAPbI_3$ film by measuring the slope. The slope of the fitting line is about 0.3417, corresponding to the activation energy E_a for about 29 meV, which is slightly smaller than the value of E_a for the $MAPbI_3$ film (Figure S8). The temperature quenching of the PL intensity is due to the exciton thermal dissociation;[33] the activation energy E_a therefore is closely matched to the exciton binding energy, which is about 29 meV for the $FAPbI_3$ film. This value is higher than that obtained from the temperature-dependent PL analysis in recent reports, which probably stems from the differences in the film parameters such as grains dimension distribution and orientation.[6,39] The exciton binding energies for the $FAPbI_3$ and $MAPbI_3$ film are both comparable to the thermal kinetic energy of ∼26 meV at room temperature, declaring the coexistence of free carriers and excitons. The fundamental nature of excited state species in these $FAPbI_3$ and $MAPbI_3$ film is more like free carriers under low excitation regime but dominant by geminate recombination at high excitation regime.[40]

In addition, the line width of PL spectra in $FAPbI_3$ gradually broaden from 160 to 340 K as clearly shown in Figure 4a, which is attributed to electron−phonon coupling.[39,41] To establish qualitatively which electron−phonon scattering mechanisms dominate in $FAPbI_3$, the line broadening of the band-edge PL emission for both compounds was measured as a function of temperature to determine the phonon energy, Γ_{ph}. The temperature dependence of peak width for excitonic peaks was analyzed using Toyozawa's equation:[42,43]

$$\Gamma(T) = \frac{A}{\exp\left(\frac{\Gamma_{ph}}{k_B T}\right) - 1} + C \quad (1)$$

DOI: 10.1021/acs.jpcc.7b02101
J. Phys. Chem. C 2017, 121, 15318−15325

where $\Gamma(T)$ is the fwhm and C is a constant line width at low temperatures due to the absence of phonon broadening. From the analysis of spectral data shown in Figure 4c using eq 1, a phonon energy Γ_{ph} of about 0.019 eV was calculated for $FAPbI_3$ and 0.026 eV for $MAPbI_3$ (Figure S9), which is close to the value reported in other study.[41] Furthermore, as shown in Figure 4a, from 160 to 340 K, the PL spectra peaks in $FAPbI_3$ all continually red-shift because the band gap decreases with increasing temperature.[33] The decrease tends to vary linearly with temperature above phase transition temperature. The energy of the PL peak changes almost linearly with the temperature as shown in Figure 4d. The continuous blue-shift for temperatures higher than 160 K can be described by a temperature coefficient $\alpha = \partial E/\partial T = 0.426$ meV/K. This counterintuitive blue-shift was also observed in lead/copper chalcogenide semiconductors like PbS(Se/Te) and CuCl(Br/I).[44]

To further identify the underlying recombination mechanisms in these hybrid perovskites, the dependence of photoluminescence on pump power was studied. The low-temperature PL from compound semiconductors with reasonably good crystalline quality is dominated by near-band-edge photoluminescence (NBEPL). It has been stated that the underlying recombination process can be identified from the behavior of the PL intensity as the excitation power is varied. As a general result, it has been found that the luminescence intensity I of the NBEPL emission lines is proportional to L^k, where L is the power of the exciting laser radiation and $1 < k < 2$ for exciton-like transition and $k < 1$ for free-to-bound and donor–acceptor pair transitions.[38,43,45] To investigate this further, we made a more comprehensive study of the excitation density dependence of the PL intensity at 80 and 293 K. As shown in Figure 5a, at the excitation density ranging from 10^{16} to 2×10^{18} cm^{-3}, the straight lines are linear regressions for $FAPbI_3$ film. A purely linear behavior is characterized by a slope of about 0.96 at 80 K. However, the behavior is then superlinear with the slope increasing to 1.21 at 293 K. For $MAPbI_3$, $k = 1.2$ at 80 K and $k = 1.51$ at 293 K shown in Figure 5b. The value of $k = 1.21$ at room temperature for $FAPbI_3$ is expected for free exciton transitions since their intensity is directly proportional to the total number of excitons, which is proportional to the excitation densities. Thus, it is concluded that the power-dependent PL measurements indicate that the PL recombination mechanism for $FAPbI_3$ is excitonic in nature at intermediate excitation densities at room temperature, coinciding with the above-mentioned results, which is perceived as one of the reasons that $FAPbI_3$ possesses excellent lasing properties.

4. CONCLUSIONS

In summary, the ASE emission in organolead halide perovskite $FAPbI_3$ film has been investigated. Compared to $MAPbI_3$, $FAPbI_3$ possesses lower threshold and higher stability derived from its low trap density and high thermal stability, which makes it more suitable for the CW pumped lasers or electrically driven lasers. We further demonstrate tunable perovskite lasing in wider wavelength region from FA-based lead halide perovskite alloys through halogen substitutions. In addition, temperature-dependent PL experiments revealed an exciton binding energy of 29 meV and optical phonon energy of 19 meV, indicating an excitonic emission in nature at room temperature. Our results provide useful insights into the optical properties of such important hybrid perovskites, promoting their future applications in optoelectronic devices.

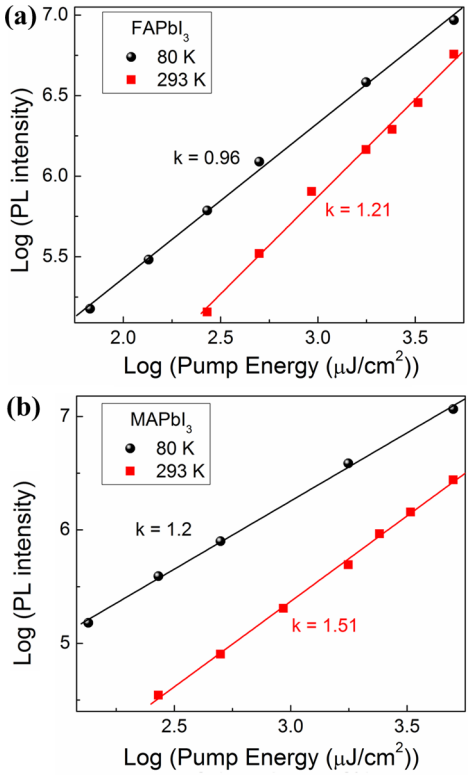

Figure 5. A log–log plot of the pump energy versus the integrated PL intensity at different temperatures for (a) $FAPbI_3$ film and (b) $MAPbI_3$ film. The solid lines are linear regressions.

■ ASSOCIATED CONTENT

Supporting Information

The Supporting Information is available free of charge on the ACS Publications website at DOI: 10.1021/acs.jpcc.7b02101.

SEM, Abs, and PL spectrum of $MAPbI_3$, schematic configuration, SEM of $(MA,FA)Pb(Br,I)_3$, wavelength-tunable SE and ASE, spectra of the MABr-stabilized $FAPbI_3$ film, temperature-dependent PL spectra, activation energy and phonon energy for $MAPbI_3$ (PDF)

■ AUTHOR INFORMATION

Corresponding Author

*E-mail: zhaoxinwu@mail.xjtu.edu.cn (Z.W.).

ORCID

Zhaoxin Wu: 0000-0003-2979-3051

Author Contributions

F.Y. and Z.W. contributed equally to the work.

Notes

The authors declare no competing financial interest.

■ ACKNOWLEDGMENTS

This work was financially supported by Basic Research Program of China (2013CB328705), National Natural Science Foundation of China (Grant No. 61275034), and Ph.D. Programs Foundation of Ministry of Education of China (Grant No. 20130201110065). The SEM work was done at International Center for Dielectric Research (ICDR), Xi'an Jiaotong

University, Xi'an, China; the authors also thank Ms. Dai for her help in using SEM.

REFERENCES

(1) Jung, H. S.; Park, N. G. Perovskite Solar Cells: From Materials to Devices. *Small* **2015**, *11*, 10−25.

(2) Sum, T. C.; Mathews, N. Advancements in Perovskite Solar Cells: Photophysics behind the Photovoltaics. *Energy Environ. Sci.* **2014**, *7*, 2518−2534.

(3) Stranks, S. D.; Snaith, H. J. Metal-Halide Perovskites for Photovoltaic and Light-Emitting Devices. *Nat. Nanotechnol.* **2015**, *10*, 391−402.

(4) Veldhuis, S. A.; Boix, P. P.; Yantara, N.; Li, M.; Sum, T. C.; Mathews, N.; Mhaisalkar, S. G. Perovskite Materials for Light-Emitting Diodes and Lasers. *Adv. Mater.* **2016**, *28*, 6804−6834.

(5) Sutherland, B. R.; Sargent, E. H. Perovskite Photonic Sources. *Nat. Photonics* **2016**, *10*, 295−302.

(6) Colella, S.; Mazzeo, M.; Rizzo, A.; Gigli, G.; Listorti, A. The Bright Side of Perovskites. *J. Phys. Chem. Lett.* **2016**, *7*, 4322−4334.

(7) Kojima, A.; Teshima, K.; Shirai, Y.; Miyasaka, T. Organometal Halide Perovskites as Visible-Light Sensitizers for Photovoltaic Cells. *J. Am. Chem. Soc.* **2009**, *131*, 6050−6051.

(8) Zhou, H.; Chen, Q.; Li, G.; Luo, S.; Song, T. B.; Duan, H. S.; Hong, Z.; You, J.; Liu, Y.; Yang, Y. Interface Engineering of Highly Efficient Perovskite Solar Cells. *Science* **2014**, *345*, 542−546.

(9) Yang, W. S.; Noh, J. H.; Jeon, N. J.; Kim, Y. C.; Ryu, S.; Seo, J.; Seok, S. I. High-Performance Photovoltaic Perovskite Layers Fabricated through Intramolecular Exchange. *Science* **2015**, *348*, 1234−1237.

(10) Xing, G.; Mathews, N.; Sun, S.; Lim, S. S.; Lam, Y. M.; Gratzel, M.; Mhaisalkar, S.; Sum, T. C. Long-range Balanced Electron- and Hole-Transport Lengths in Organic-Inorganic $CH_3NH_3PbI_3$. *Science* **2013**, *342*, 344−347.

(11) Stranks, S. D.; Eperon, G. E.; Grancini, G.; Menelaou, C.; Alcocer, M. J. P.; Leijtens, T.; Herz, L. M.; Petrozza, A.; Snaith, H. J. Electron-Hole Diffusion Lengths Exceeding 1 Micrometer in an Organometal Trihalide Perovskite Absorber. *Science* **2013**, *342*, 341−344.

(12) Zhao, Y.; Nardes, A. M.; Zhu, K. Solid-State Mesostructured Perovskite $CH_3NH_3PbI_3$ Solar Cells: Charge Transport, Recombination, and Diffusion Length. *J. Phys. Chem. Lett.* **2014**, *5*, 490−494.

(13) NREL, 2016; http://www.nrel.gov/ncpv/images/efficiency_chart.jpg, accessed April 2016.

(14) Deschler, F.; Price, M.; Pathak, S.; Klintberg, L. E.; Jarausch, D. D.; Higler, R.; Huttner, S.; Leijtens, T.; Stranks, S. D.; Snaith, H. J.; et al. High Photoluminescence Efficiency and Optically Pumped Lasing in Solution-Processed Mixed Halide Perovskite Semiconductors. *J. Phys. Chem. Lett.* **2014**, *5*, 1421−1426.

(15) Xing, G. C.; Mathews, N.; Lim, S. S.; Yantara, N.; Liu, X. F.; Sabba, D.; Gratzel, M.; Mhaisalkar, S.; Sum, T. C. Low-Temperature Solution-Processed Wavelength-Tunable Perovskites for Lasing. *Nat. Mater.* **2014**, *13*, 476−480.

(16) Yuan, F.; Wu, Z.; Dong, H.; Xia, B.; Xi, J.; Ning, S.; Ma, L.; Hou, X. Electric Field-Modulated Amplified Spontaneous Emission in Organo-Lead Halide Perovskite $CH_3NH_3PbI_3$. *Appl. Phys. Lett.* **2015**, *107*, 261106.

(17) Suarez, I.; Juarez-Perez, E. J.; Bisquert, J.; Mora-Sero, I.; Martinez-Pastor, J. P. Polymer/Perovskite Amplifying Waveguides for Active Hybrid Silicon Photonics. *Adv. Mater.* **2015**, *27*, 6157−6162.

(18) Zhang, Q.; Ha, S. T.; Liu, X. F.; Sum, T. C.; Xiong, Q. H. Room-Temperature Near-Infrared High-Q Perovskite Whispering-Gallery Planar Nano lasers. *Nano Lett.* **2014**, *14*, 5995−6001.

(19) Liao, Q.; Hu, K.; Zhang, H.; Wang, X.; Yao, J.; Fu, H. Perovskite Microdisk Microlasers Self-Assembled from Solution. *Adv. Mater.* **2015**, *27*, 3405−3410.

(20) Protesescu, L.; Yakunin, S.; Kumar, S.; Bar, J.; Bertolotti, F.; Masciocchi, N.; Guagliardi, A.; Grotevent, M.; Shorubalko, I.; Bodnarchuk, M. I.; et al. Dismantling the "Red Wall" of Colloidal Perovskites: Highly Luminescent Formamidinium and Formamidinium-Cesium Lead Iodide Nanocrystals. *ACS Nano* **2017**, *11*, 3119−3134.

(21) Zhu, H.; Fu, Y.; Meng, F.; Wu, X.; Gong, Z.; Ding, Q.; Gustafsson, M. V.; Trinh, M. T.; Jin, S.; Zhu, X. Y. Lead Halide Perovskite Nanowire Lasers with Low Lasing Thresholds and High Quality Factors. *Nat. Mater.* **2015**, *14*, 636−642.

(22) Xing, J.; Liu, X. F.; Zhang, Q.; Ha, S. T.; Yuan, Y. W.; Shen, C.; Sum, T. C.; Xiong, Q. Vapor Phase Synthesis of Organometal Halide Perovskite Nanowires for Tunable Room-Temperature Nanolasers. *Nano Lett.* **2015**, *15*, 4571−4577.

(23) Fu, Y.; Zhu, H.; Schrader, A. W.; Liang, D.; Ding, Q.; Joshi, P.; Hwang, L.; Zhu, X. Y.; Jin, S. Nanowire Lasers of Formamidinium Lead Halide Perovskites and Their Stabilized Alloys with Improved Stability. *Nano Lett.* **2016**, *16*, 1000−1008.

(24) Saliba, M.; Wood, S. M.; Patel, J. B.; Nayak, P. K.; Huang, J.; Alexander-Webber, J. A.; Wenger, B.; Stranks, S. D.; Horantner, M. T.; Wang, J. T.; et al. Structured Organic-Inorganic Perovskite toward a Distributed Feedback Laser. *Adv. Mater.* **2016**, *28*, 923−929.

(25) Fang, H.-H.; Wang, F.; Adjokatse, S.; Zhao, N.; Loi, M. A. Photoluminescence Enhancement in Formamidinium Lead Iodide Thin Films. *Adv. Funct. Mater.* **2016**, *26*, 4653−4659.

(26) Cadelano, M.; Sarritzu, V.; Sestu, N.; Marongiu, D.; Chen, F.; Piras, R.; Corpino, R.; Carbonaro, C. M.; Quochi, F.; Saba, M.; et al. Can Trihalide Lead Perovskites Support Continuous Wave Lasing? *Adv. Opt. Mater.* **2015**, *3*, 1557−1564.

(27) Stoumpos, C. C.; Malliakas, C. D.; Kanatzidis, M. G. Semiconducting Tin and Lead Iodide Perovskites with Organic Cations: Phase Transitions, High Mobilities, and Near-Infrared Photoluminescent Properties. *Inorg. Chem.* **2013**, *52*, 9019−9038.

(28) Binek, A.; Hanusch, F. C.; Docampo, P.; Bein, T. Stabilization of the Trigonal High-Temperature Phase of Formamidinium Lead Iodide. *J. Phys. Chem. Lett.* **2015**, *6*, 1249−1253.

(29) Bi, C.; Shao, Y.; Yuan, Y.; Xiao, Z.; Wang, C.; Gao, Y.; Huang, J. Understanding the Formation and Evolution of Interdiffusion Grown Organolead Halide Perovskite Thin Films by Thermal Annealing. *J. Mater. Chem. A* **2014**, *2*, 18508−18514.

(30) Dai, J.; Fu, Y. P.; Manger, L. H.; Rea, M. T.; Hwang, L.; Goldsmith, R. H.; Jin, S. Carrier Decay Properties of Mixed Cation Formamidinium-Methylammonium Lead Iodide Perovskite $[HC(NH_2)_2]_{1-x}[CH_3NH_3]_xPbI_3$ Nanorods. *J. Phys. Chem. Lett.* **2016**, *7*, 5036−5043.

(31) Hoke, E. T.; Slotcavage, D. J.; Dohner, E. R.; Bowring, A. R.; Karunadasa, H. I.; McGehee, M. D. Reversible Photo-Induced Trap Formation in Mixed-Halide Hybrid Perovskites for Photovoltaics. *Chem. Sci.* **2015**, *6*, 613−617.

(32) Fabini, D. H.; Stoumpos, C. C.; Laurita, G.; Kaltzoglou, A.; Kontos, A. G.; Falaras, P.; Kanatzidis, M. G.; Seshadri, R. Reentrant Structural and Optical Properties and Large Positive Thermal Expansion in Perovskite Formamidinium Lead Iodide. *Angew. Chem., Int. Ed.* **2016**, *55*, 15392−15396.

(33) D'Innocenzo, V.; Grancini, G.; Alcocer, M. J. P.; Kandada, A. R. S.; Stranks, S. D.; Lee, M. M.; Lanzani, G.; Snaith, H. J.; Petrozza, A. Excitons versus Free Charges in Organo-Lead Tri-Halide Perovskites. *Nat. Commun.* **2014**, *5*, 3586.

(34) Kao, T. S.; Chou, Y. H.; Chou, C. H.; Chen, F. C.; Lu, T. C. Lasing Behaviors upon Phase Transition in Solution-Processed Perovskite Thin Films. *Appl. Phys. Lett.* **2014**, *105*, 231108.

(35) Wehrenfennig, C.; Liu, M.; Snaith, H. J.; Johnston, M. B.; Herz, L. M. Charge Carrier Recombination Channels in the Low-Temperature Phase of Organic-Inorganic Lead Halide Perovskite Thin Films. *APL Mater.* **2014**, *2*, 081513.

(36) Dai, J.; Zheng, H. G.; Zhu, C.; Lu, J. F.; Xu, C. X. Comparative Investigation on Temperature-Dependent Photoluminescence of $CH_3NH_3PbBr_3$ and $CH(NH_2)_2PbBr_3$ Microstructures. *J. Mater. Chem. C* **2016**, *4*, 4408−4413.

(37) Leroux, M.; Grandjean, N.; Beaumont, B.; Nataf, G.; Semond, F.; Massies, J.; Gibart, P. Temperature Quenching of Photoluminescence Intensities in Undoped and Doped GaN. *J. Appl. Phys.* **1999**, *86*, 3721.

DOI: 10.1021/acs.jpcc.7b02101
J. Phys. Chem. C 2017, 121, 15318−15325

(38) Luckert, F.; Yakushev, M. V.; Faugeras, C.; Karotki, A. V.; Mudryi, A. V.; Martin, R. W. Excitation Power and Temperature Dependence of Excitons in $CuInSe_2$. *J. Appl. Phys.* **2012**, *111*, 093507.
(39) Fang, H.-H.; Wang, F.; Adjokatse, S.; Zhao, N.; Even, J.; Antonietta Loi, M. Photoexcitation Dynamics in Solution-Processed Formamidinium Lead Iodide Perovskite Thin Films for Solar Cell Applications. *Light: Sci. Appl.* **2015**, *5*, e16056.
(40) Manger, L. H.; Rowley, M. B.; Fu, Y. P.; Foote, A. K.; Rea, M. T.; Wood, S. L.; Jin, S.; Wright, J. C.; Goldsmith, R. H. Global Analysis of Perovskite Photophysics Reveals Importance of Geminate Pathways. *J. Phys. Chem. C* **2017**, *121*, 1062−1071.
(41) Wright, A. D.; Verdi, C.; Milot, R. L.; Eperon, G. E.; Pérez-Osorio, M. A.; Snaith, H. J.; Giustino, F.; Johnston, M. B.; Herz, L. M. Electron−Phonon Coupling in Hybrid Lead Halide Perovskites. *Nat. Commun.* **2016**, *7*, 11755.
(42) Youn, C. J.; Jeong, T. S.; Han, M. S.; Kim, J. H. Optical Properties of Zn-Terminated ZnO Bulk. *J. Cryst. Growth* **2004**, *261*, 526−532.
(43) Sebastian, M.; Peters, J. A.; Stoumpos, C. C.; Im, J.; Kostina, S. S.; Liu, Z.; Kanatzidis, M. G.; Freeman, A. J.; Wessels, B. W. Excitonic Emissions and Above-Band-Gap Luminescence in the Single-Crystal Perovskite Semiconductors $CsPbBr_3$ and $CsPbCl_3$. *Phys. Rev. B: Condens. Matter Mater. Phys.* **2015**, *92*, 235210.
(44) Dey, P.; Paul, J.; Bylsma, J.; Karaiskaj, D.; Luther, J. M.; Beard, M. C.; Romero, A. H. Origin of the Temperature Dependence of the Band Gap of PbS and PbSe Quantum Dots. *Solid State Commun.* **2013**, *165*, 49−54.
(45) Le Ru, E. C.; Fack, J.; Murray, R. Temperature and Excitation Density Dependence of the Photoluminescence from Annealed InAs/GaAs Quantum Dots. *Phys. Rev. B: Condens. Matter Mater. Phys.* **2003**, *67*, 245318.

DOI: 10.1021/acs.jpcc.7b02101
J. Phys. Chem. C 2017, 121, 15318−15325